

## Effect of Aging Treatment on the Electrochemical and Corrosion Behavior of NiTiRe Shape Memory Alloy

Nader El-Bagoury<sup>1,2</sup>, Mohammed A. Amin<sup>1,3\*</sup>, Murat Saracoglu<sup>4</sup>

<sup>1</sup> TAIF University, Chemistry Department, Faculty of Science, P.O. Box 888, El-Haweyah, Saudia Arabia

<sup>2</sup> Central Metallurgical Research and Development Institute, CMRDI, Casting Technology Lab., Manufacturing Technology Dept., P.O. Box 87, Helwan, Cairo, Egypt

<sup>3</sup> Department of Chemistry, Faculty of Science, Ain Shams University, 11566 Abbassia, Cairo, Egypt

<sup>4</sup> Faculty of Education, Erciyes University, 38039 Kayseri, Turkey

\*E-mail: [maaismail@yahoo.com](mailto:maaismail@yahoo.com)

Received: 26 January 2015 / Accepted: 3 May 2015 / Published: 27 May 2015

---

In this study, Ni<sub>52</sub>Ti<sub>47.7</sub>Re<sub>0.3</sub> shape memory alloy was subjected to solution treatment at 1000 °C for 24h (the tested alloy), followed by ageing at 300, 400, 500 and 600 °C for 3h. The objective is to investigate the effect of ageing temperature on the uniform and pitting corrosion characteristics of Ni<sub>52</sub>Ti<sub>47.7</sub>Re<sub>0.3</sub> alloy. Measurements were conducted in 1.0 M H<sub>2</sub>SO<sub>4</sub> solutions without and with 0.2 M NH<sub>4</sub>F, using polarization, impedance, and chronoamperometry measurements. Morphologies of the corroded surfaces were examined by SEM/EDX examinations. Results obtained from the employed electrochemical techniques were in good agreement and showed that the rates of the uniform and pitting corrosion processes of the tested alloy decrease with increase in the aging temperature, reaching their minimum values at an aging temperature of 400 °C. Further increase in the aging temperature up to 600 °C led to an obvious increase in the rates of corrosion. Experimental findings were interpreted adopting the effect of the aging temperature on the microstructure of the tested alloy.

---

**Keywords:** NiTiRe Shape memory alloys; Aging; Microstructure; Corrosion behavior

### 1. INTRODUCTION

A shape memory alloy (SMA) or “smart alloy” is able to memorize and recover its original shape, after it has been deformed by heating over its transformation temperature. This unique effect of returning to an original geometry after a large inelastic deformation (near 10%) is known as the shape memory effect (SME), that was first discovered by Arne Ölander in 1932 [1], and the term “shape-memory” was first described by Vernon in 1941 [2] for his polymeric dental material. The importance of shape memory materials (SMMs) was not recognized until William Buehler and Frederick Wang

revealed the shape memory effect (SME) in a nickel-titanium (NiTi) alloy in 1962 [3,4], which is also known as nitinol (derived from the material composition and the place of discovery, i.e. a combination of NiTi and Naval Ordnance Laboratory). Since then, the demand for SMAs for engineering and technical applications has been increasing in numerous commercial fields; such as in consumer products and industrial applications [5–7], structures and composites [8], automotive [9,10], aerospace [11–14], mini actuators and micro-electromechanical systems (MEMS) [13,15–18], robotics [19–21], and even in fashion [22].

Although iron-based and copper-based SMAs, such as Fe–Mn–Si, Cu–Zn–Al and Cu–Al–Ni, are low-cost and commercially available, due to their instability, impracticability (e.g. brittleness) [23–25] and poor thermo-mechanic performance [26]; NiTi SMA is much more preferable for most applications, and is one of the most important engineering materials. However, each material has their own advantage for particular requirements or applications [26].

NiTi alloys are also important materials for biomedical and dental devices because of their unique properties, comparatively high corrosion resistance and good biocompatibility [13,15,27–32]. The good corrosion resistance of NiTi results from the formation of very stable, continuous, highly adherent, and protective oxide films on its surface [33]. Because titanium is highly reactive and has a high affinity for oxygen, these beneficial surface oxide films form spontaneously when fresh metal surfaces are exposed to air and/or moisture. In fact, a damaged oxide film can generally heal itself if at least traces of oxygen or water (moisture) are present in the environment [33]. These materials are therefore in a passive state at the open-circuit potential. The passive films act as an effective barrier to separate the substrate alloys from the corrosive environment and thus protects the substrate alloys from further corrosion processes [34–36]. Unfortunately, the passive film does not afford complete protection of the substrate alloys. For instance, in tribocorrosion systems, tribological contact can often damage or even remove the passive film, as a result, exposing the active substrate alloy surface to the corrosive environment, resulting in an anodic dissolution of the alloys. In addition, certain aggressive anions, such as  $\text{Cl}^-$  and  $\text{F}^-$  can also induce passivity breakdown, resulting in various forms of localized corrosion, such as pitting attack and stress corrosion cracking [37–40]. Localized corrosion processes can result in the rapid penetration of a cavity pit or crack into the alloy substrate, thus leading to premature failure. Acid media can also result in corrosion attack. It is a challenge to develop new materials having desired anti-corrosion properties to be used as an engineering moving part in acid environment [41–44].

Considering the potential applications of NiTi SMAs, studying the corrosion behavior of such materials is an important parameter for investigation, particularly the generalized corrosion attack occurring in acid media, due to the aggressive environments where these alloys are used. Furthermore, the literature contains very few studies about the corrosion behavior, corrosion rate, and anodic behavior in acid media of these materials. Although many research projects have been recently conducted on the corrosion behavior of NiTi SMAs, as we previously clarified, the data are far from sufficient. For instance, little seems to be published regarding the effects of alloying elements on the corrosion behavior of NiTi SMAs [45–47]. Recently, we have studied the effect of alloying a NiTi SMA with Re [48] and Co [49], and the obtained results showed that the presence of Re and Co

enhanced the corrosion resistance of the tested SMA to an extent depending on their abundance in the alloy.

The understanding of corrosion behavior in NiTi is critical for the devices using this shape-memory alloy. The present work is the extension of the previous study recently published by our research group [50,51], in which  $\text{Ni}_{52}\text{Ti}_{47.7}\text{Re}_{0.3}$  alloy was solution treated at 1000 °C for 24 h then aged at various temperatures of 300, 400, 500 and 600 °C for 3 h, and the microstructure, martensitic transformation and mechanical properties of that alloy was investigated as a function of aging temperature [50]. The Results showed that the microstructure of the solution treated alloy consists of martensite as a parent phase and some precipitates of  $\text{Ti}_2\text{Ni}$  phase. The aged alloys had a microstructure as same as that of solution treated alloy in addition to the existence of other types of precipitation like  $\text{Ni}_4\text{Ti}_3$  and  $\text{Ni}_3\text{Ti}$  [50,51].

The objective here is to explore the effect of aging temperature on the uniform and pitting corrosion characteristics of  $\text{Ni}_{52}\text{Ti}_{47.7}\text{Re}_{0.3}$  SMA in 1.0 M  $\text{H}_2\text{SO}_4$  solutions without and with 0.2 M  $\text{NH}_4\text{F}$ , employing various electrochemical techniques. Morphologies of the pitted surfaces were studied by SEM/EDX examinations as a function of the aging temperature. Based on the experimental findings of the present work, together with those performed in our lab and recently published [50,51], the optimum heat treatment condition for our tested  $\text{Ni}_{52}\text{Ti}_{47.7}\text{Re}_{0.3}$  SMA with comprehensive corrosion and mechanical properties could be obtained.

## 2. EXPERIMENTAL

Polycrystalline  $\text{Ni}_{52}\text{Ti}_{47.7}\text{Re}_{0.3}$  shape memory alloy was manufactured by melting pure elements (> 99.99% purity) in an induction vacuum furnace. The alloy was melted four times to ensure homogeneity and cast into an investment casting ceramic mold. This mold was preheated to 1000 °C before pouring process. These investigated alloys were solutionized at 1000 °C for 24 h followed by quenching in iced water. The aging process was carried out at various temperatures ranging from 300 to 600 °C for 3 h then iced water quenching. The microstructure of solutionized and aged alloys was previously studied [50,51].

Plates of size 1.0 cm x 1.0 cm x 0.1 cm have been used in this work. Before each run, the plates were wet ground with #600-grit silicon carbide (SiC) paper, thoroughly washed and ultrasonically cleaned in deionized water and absolute ethanol, for 10 min, dried in air, and finally immersed in the electrochemical cell. The samples were then subjected to open circuit conditions until a steady state potential was reached. This procedure was accomplished in 120 min and the potential value obtained was close to the corrosion potential ( $E_{\text{corr}}$ ) derived from polarization measurements.

The square plates were connected as the working electrodes in stagnant naturally aerated 1.0 M  $\text{H}_2\text{SO}_4$  solutions without and with 0.2 M  $\text{NH}_4\text{F}$ . Only one side of the specimen was in contact with the electrolyte. The remaining side was coated by a nonreactive and non-conductive varnish. Electrochemical studies were performed using a thermostated double jacket glass cell in the conventional three-electrode configuration. The potential of the working electrode was measured against the saturated calomel reference electrode (SCE, +0.240 V (SHE)). The reference electrode was inserted into a Luggin Capillary. The counter electrode was a platinum-coil. The electrochemical cell

had a volume of 200 mL, large enough to avoid significant drifts in composition during the experiments. The electrochemical cell was connected to a potentiostat; Autolab frequency response analyzer (FRA) coupled to an Autolab Potentiostat/Galvanostat (PGSTAT30) with FRA2 module connected to a personal computer.

The electrochemical methods employed to study the uniform corrosion behavior of the tested alloy as a function of the aging temperature include: (i) monitoring the open circuit potential (OCP) up 2.0 hrs, (ii) EIS measured at the respective corrosion potential ( $E_{\text{corr}}$ ), and (iii) polarization measurements around  $E_{\text{corr}}$  ( $E_{\text{corr}} \pm 250$  mV). Impedance measurements were carried out using AC signals of amplitude 5 mV peak to peak at the open circuit potential in the frequency range 100 kHz to 0.1 Hz. For polarization studies around  $E_{\text{corr}}$ , the potential of the working electrode is varied from ( $E_{\text{corr}} - 0.25$ )V vs. SCE to ( $E_{\text{corr}} + 0.25$ )V vs. SCE using a scan rate of  $0.167 \text{ mV s}^{-1}$ .

Potentiodynamic anodic polarization and chronoamperometry measurements were employed for investigating the effect of the aging temperature on the anodic behavior of the tested alloy. This includes passivity (passive layer formation and growth) and breakdown of passivity induced by  $\text{F}^-$  (kinetics of pit nucleation and propagation). The potentiodynamic polarization measurements were carried out at a scan rate of  $2.0 \text{ mV s}^{-1}$ , starting from a cathodic potential of  $-2.0 \text{ V}$  up to an anodic potential of  $2.0 \text{ V}$ .

The order of performing electrochemical measurements was: (i) Chronopotentiometry (zero current); OCP vs. time (up to 2hrs), followed by (ii) impedance measurements at  $E_{\text{corr}}$ , then (iii) polarization measurements around  $E_{\text{corr}}$  ( $E_{\text{corr}} \pm 250$  mV). As the later is a destructive technique, the cell is cleaned, the test solution is replaced by a fresh one, and a cleaned set of electrodes was used for (iv) potentiodynamic anodic polarization measurements. Finally, chronoamperometry measurements were carried out in a cleaned cell with a fresh test solution and a cleaned set of electrodes using a two step procedure, namely: the working electrode was first held at the starting potential for 60s to attain a reproducible electroreduced electrode surface. Then the electrode was held at constant anodic potential ( $E_a$ ), where the anodic current was recorded as a function of time.

For corrosion rates evaluated by ICP-AES method of chemical analysis, the  $\text{Ni}^{2+}$  ions concentration was determined for the tested alloy as a function of the aged temperature in a  $1.0 \text{ M H}_2\text{SO}_4$  solution after an immersion time of 96 h. This has occurred according to the ASTM G31–72(2004) standard, using Perkin–Elmer Optima 2100 Dual View inductively coupled plasma atomic emission spectrometry (ICP-AES) instrument connected with AS 93 Plus autosampler.

Morphologies of the corroded surfaces were investigated using an Analytical Scanning Electron Microscope JEOL JSM 6390 LA. The compositions of such corroded surfaces were determined using ZAF software to quantify the energy-dispersive X-ray spectroscopy (EDS) spectra obtained by an EDS attachment (JEOL EDS EX-54175JMU) on the JEOL SEM.

### 3. RESULTS AND DISCUSSION

#### 3.1. Open-circuit potential vs. time measurements

The open-circuit potential (OCP) of the tested alloy (that is solutionized at  $1000 \text{ }^\circ\text{C}$ , but not yet aged) is monitored up to 2 h of immersion in  $1.0 \text{ M H}_2\text{SO}_4$  solutions at  $25 \text{ }^\circ\text{C}$  as a function of the

temperature of the aging treatment, Fig. 1. It can be seen for all cases that in the first moments of immersion, the OCP moves rapidly towards less negative values due to the initial formation and growth of a passive oxide film (passivation).

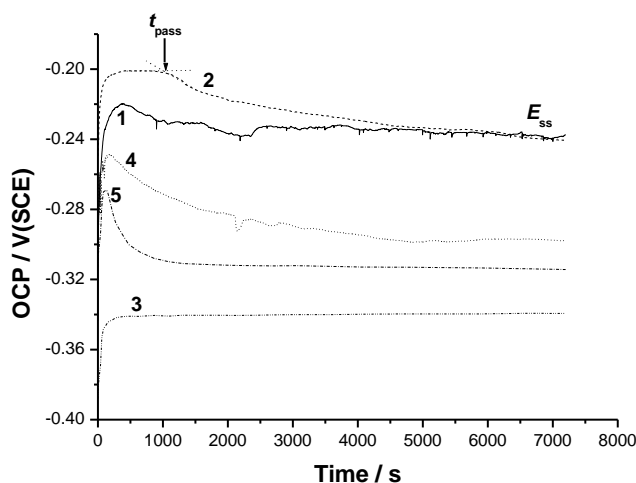


**Figure 1.** Open-circuit potential (OCP) vs. time plots recorded for Ni<sub>52</sub>Ti<sub>47.7</sub>Re<sub>0.3</sub> shape memory alloy in 1.0 M H<sub>2</sub>SO<sub>4</sub> solutions at 25 °C as a function of the temperature of the aging treatment. The alloy is first solution treated at 1000 °C for 24h (curve 1), then aged at various temperatures of 300, 400, 500 and 600 °C for 3h, curves 2-5, respectively.

After a certain time (designated here as the life-time of the passivation process,  $t_{\text{pass}}$ ), depending on the aging temperature, the potential declined to a reasonably steady value,  $E_{\text{ss}}$ . This trend indicated the occurrence of two counter-acting processes. The first process being passivation of the alloy surface, and consequently delayed-action corrosion occurred shifting the OCP to nobler values. The second process is depassivation (corrosion), which dragged the potential back towards active values [48]. The competition between these two counter-acting processes may explain the appearance of an arrest in the OCP vs. time curves of Fig. 1, particularly when the alloy is aged at temperatures 500 °C and 600 °C (curves 4 and 5, respectively).

It follows from Fig. 1 that the value and location of potential maximum ( $t_{\text{pass}}$ ) and the slope of the potential decay following  $t_{\text{pass}}$  depend on the temperature of the aging treatment. The values of  $t_{\text{pass}}$  are always longer when the alloy is aged at 300 °C (curve 2) and 400 °C (curve 3), and get shorter upon increasing the aging temperature further to 500 °C (curve 4) and 600 °C (curve 5). The slope of the potential decay following  $t_{\text{pass}}$  obviously enhances when the tested alloy is aged at 500 °C (curve 4) and 600 °C (curve 5). On the other hand, it is markedly ceased and completely prevented upon aging the alloy at 300 °C and 400 °C, as shown in curves 2 and 3, respectively.

These findings give us an initial impression that the surface of our tested alloy is expected to be subjected to corrosion when aged at 500 °C and 600 °C much more than when aged at 300 °C and 400 °C, with that aged at 400 °C being the best as it stabilizes readily in these solutions (see curve 3). Further inspection of Fig. 1 reveals that the steady-state potential varies with the aging temperature, but with no definite trend. However, the steady-state potential is found to correspond to the free corrosion potential,  $E_{\text{corr}}$  of the alloy, as confirmed from polarization studies, *vide infra*.

### 3.2. Monitoring rates of uniform corrosion

#### 3.2.1. Polarization measurements

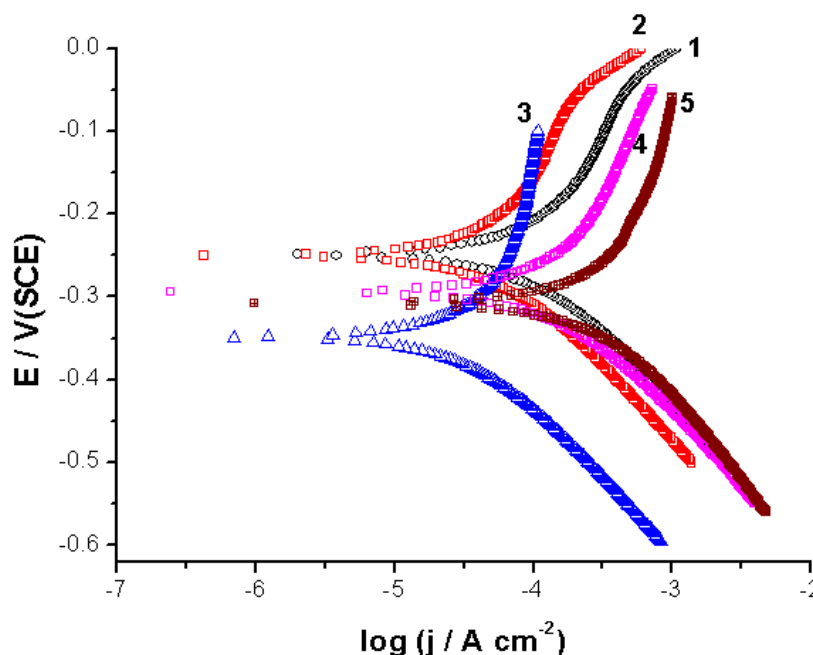


**Figure 2.** Cathodic and anodic polarization curves recorded for  $\text{Ni}_{52}\text{Ti}_{47.7}\text{Re}_{0.3}$  shape memory alloy in 1.0 M  $\text{H}_2\text{SO}_4$  solutions at a scan rate of  $0.167 \text{ mV s}^{-1}$  at  $25^\circ\text{C}$  as a function of the temperature of the aging treatment. The alloy is first solution treated at  $1000^\circ\text{C}$  for 24h (curve 1), then aged at various temperatures of 300, 400, 500 and  $600^\circ\text{C}$  for 3h, curves 2-5, respectively.

Figure 2 shows the cathodic and anodic polarization curves recorded for our tested  $\text{Ni}_{52}\text{Ti}_{47.7}\text{Re}_{0.3}$  SMA in 1.0 M  $\text{H}_2\text{SO}_4$  solutions at different aging temperatures. Measurements were conducted at a scan rate of  $0.167 \text{ mV s}^{-1}$  at  $25^\circ\text{C}$ . The cathodic branch of the polarization curve represents hydrogen evolution, while the anodic one shows alloy dissolution. It is seen that, upon increasing the aging temperature from  $300^\circ\text{C}$  to  $600^\circ\text{C}$ , remarkable changes in the profile of the Tafel plots, particularly in the location of the corrosion potential ( $E_{\text{corr}}$ ) and in the magnitudes of the overpotentials of both the anodic and cathodic processes, result. There is no definite trend in the direction of variation of  $E_{\text{corr}}$  with aging temperature, but it exactly follows the direction of variation of  $E_{\text{ss}}$  observed in the OCP vs. time plots (Fig. 1). In addition, the numerical values of  $E_{\text{corr}}$  and  $E_{\text{ss}}$  are close to each other. This confirms that the steady-potential obtained from monitoring OCP (Fig.1) corresponds to the free corrosion potential of the tested alloy.

It is obvious that the anodic polarization curves do not display the expected log/linear Tafel behavior, with anodic branches exhibiting curvature over the complete applied potential range. The curvature of the anodic branch may be attributed to the deposition of the corrosion products on the alloy surface to form a non-passive surface film. The absence of linearity in anodic branches prevents linear extrapolation to  $E_{\text{corr}}$ . This in turn makes accurate evaluation of the anodic Tafel slope ( $\beta_a$ ), and hence  $j_{\text{corr}}$ , from anodic branches impossible. This was the reason why values of  $\beta_a$ , calculated from the software, were not included here. However, the cathodic branch for all tested alloys is under activation

control and exhibits linearity in accord with Tafel relationship. Values of  $j_{\text{corr}}$  were therefore estimated by Tafel extrapolation of the cathodic part of the polarization curves to  $E_{\text{corr}}$  [52]. Estimated values of  $j_{\text{corr}}$  were converted into corrosion rate (in mpy) (milli-inches/year; the penetration rate of corrosion through a metal) as per ASTM G102 – 89 [53], which is given as:

$$\text{Corrosion rate, } v = (K \times j_{\text{corr}} \times EW) / \rho \quad (1)$$

Where  $K = a$  constant given by  $3.27 \times 10^{-3}$  mm g/ $\mu\text{A}$  cm year,  $EW$  = equivalent weight of NiTi alloy in grams, and  $\rho$  = density of NiTi in g cm<sup>3</sup>, and  $j_{\text{corr}}$  is measured in  $\mu\text{A}$  cm<sup>-2</sup>.

**Table 1.** Effect of aging temperature (300-600 °C) on the electrochemical kinetic parameters and rates of corrosion (evaluated from ICP-AES and Tafel extrapolation methods) for Ni<sub>52</sub>Ti<sub>47.7</sub>Re<sub>0.3</sub> shape memory alloy heat treated at 1000 °C for 24h (the tested alloy) in 1.0 M H<sub>2</sub>SO<sub>4</sub> solutions at 25 °C. Duration of the aging process is 3h.

Alloy experimental conditions	$E_{\text{corr}}$ (V)	$j_{\text{corr}}$ (A cm <sup>-2</sup> )	$\beta_c$ (V dec <sup>-1</sup> )	$v_{\text{Tafel}}$ (mpy)	$v_{\text{ICP}}$ (mpy)
Tested alloy (without aging)	-0.255	$1.17 \times 10^{-4}$	-0.192	1.04	1.10
Tested alloy after aging @ 300 °C	-0.251	$0.6 \times 10^{-4}$	-0.186	0.54	0.60
Tested alloy after aging @ 400 °C	-0.35	$0.36 \times 10^{-4}$	-0.188	0.32	0.40
Tested alloy after aging @ 500 °C	-0.295	$2.04 \times 10^{-4}$	-0.195	1.82	2.07
Tested alloy after aging @ 600 °C	-0.31	$3.24 \times 10^{-4}$	-0.202	2.89	3.12

Table 1 collects the electrochemical parameters associated with polarization measurements for the tested alloy as a function of the aging temperature. These include  $j_{\text{corr}}$ ,  $E_{\text{corr}}$ , and cathodic Tafel slope ( $\beta_c$ ). Values of the corrosion rate evaluated from Tafel extrapolation method are also included in Table 1. It is obvious from Table 1 that the values of  $j_{\text{corr}}$ , and hence those of the corrosion rate, decreased upon increasing the aging temperature, reaching its minimum value (0.32 mpy) at an aging temperature of 400 °C, then enhanced with further increase in the aging temperature recording a corrosion rate value of 2.89 mpy at 600 °C.

### 3.2.2. ICP-AES method of chemical analysis

To further confirm the effect of the aging temperature on the uniform corrosion behavior of the tested alloy, an independent method of chemical analysis, namely ICP-AES was employed. The objective is to monitor the uniform corrosion rate of the alloy as a function of the aging temperature via determination of Ni<sup>2+</sup> in solution after each corrosion test. The amount of nickel released into the corrosive medium was taken as a measure of the corrosion rate [54]. In ICP measurements, known aliquots of the solution containing dissolved Ni<sup>2+</sup> were withdrawn at a given aging temperature after 7 days of immersion in 1.0 M H<sub>2</sub>SO<sub>4</sub> solution and analyzed. Values of the uniform corrosion rate ( $v$ ) were recorded and expressed as mg cm<sup>-2</sup> h<sup>-1</sup> (i.e., mass, in mg, of Ni dissolved as Ni<sup>2+</sup> per unit area per unit time). Each corrosion rate value was converted into its corresponding corrosion current density ( $j_{\text{corr}}$ ) value using Faraday's law, and subsequently converted into corrosion rate (in mpy), Table 1, using Equation (1). The corrosion rate values estimated from ICP (Table 1) have decreased from 1.10

mpy for the tested alloy ( $\text{Ni}_{52}\text{Ti}_{47.7}\text{Re}_{0.3}$  SMA subjected to solution treatment at 1000 °C for 24h, but not yet aged) to 0.40 mpy when the tested alloy is aged at 400 °C, then increased with further increase in the aging temperature and recorded a value of 3.12 mpy at 600 °C. Thus the alloy exhibited the highest corrosion resistance when aged at a temperature of 400 °C. These findings go parallel with polarization measurements (Fig. 2), and the agreement in the rates of corrosion between ICP-AES and Tafel extrapolation methods confirms the validity of corrosion rates measured by the later.

### 3.3. Impedance measurements

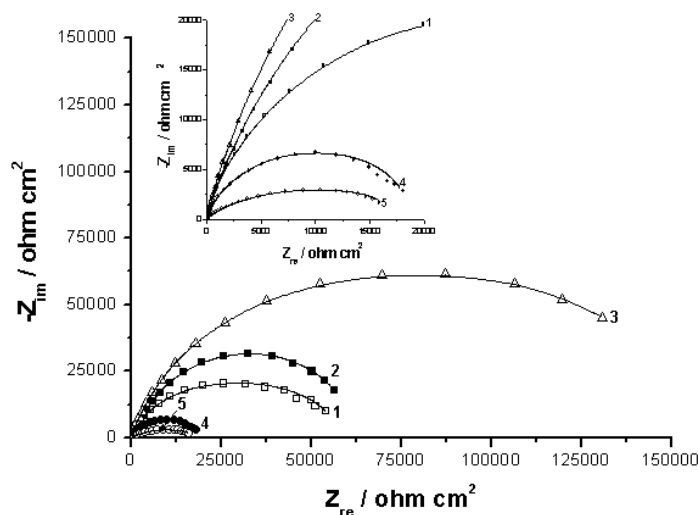


**Figure 3.** Complex-plane impedance plots recorded for  $\text{Ni}_{52}\text{Ti}_{47.7}\text{Re}_{0.3}$  shape memory alloy as a function of the aging temperature in 1.0 M  $\text{H}_2\text{SO}_4$  solutions at the respective  $E_{\text{corr}}$  at 25 °C. The alloy is first solutionized at 1000 °C for 24h (curve 1), then aged at various temperatures of 300, 400, 500 and 600 °C for 3h, curves 2-5, respectively.

In order to further explore the influence of the aging process on the corrosion resistance of  $\text{Ni}_{52}\text{Ti}_{47.7}\text{Re}_{0.3}$  alloy, EIS technique was applied. Measurements were conducted in 1.0 M  $\text{H}_2\text{SO}_4$  solutions as a function of the aging temperature at the respective  $E_{\text{corr}}$ , and the results obtained are depicted in Fig. 3. In all cases, the impedance plots are characterized by a capacitive time constant, the diameter of which is a function of the aging temperature. The capacitive impedance arc is an indication of the corrosion process under activation control [55,56]. A mathematical analysis of the impedance diagrams showed that the center of charge-transfer semicircle lies below the real axis, and that the slopes of the  $\log |Z|$  against  $\log f$  plots (not included here) are not -1. To describe this response of properly, a constant phase element, CPE, was used whose impedance,  $Z_{\text{CPE}}$ , is given by the expression [55,56]:

$$Z_{\text{CPE}} = Q^{-1}(j\omega)^{-n} \tag{2}$$

where  $Q$  is the CPE constant (a proportional factor),  $\omega$  the angular frequency (in  $\text{rad s}^{-1}$ ),  $j^2 = -1$  the imaginary number and  $n$  is the CPE exponent. The introduction of such a CPE is often used to interpret data for rough solid electrodes [57].

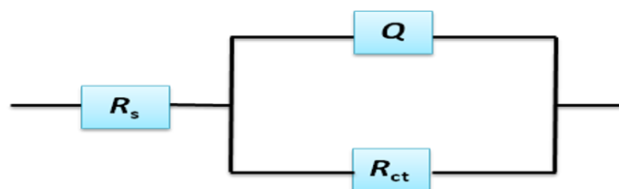


**Figure 4.** The equivalent circuit used to fit the EIS data.

**Table 2.** Effect of aging temperature (300-600 °C) on the EIS fitting parameters recorded for Ni<sub>52</sub>Ti<sub>47.7</sub>Re<sub>0.3</sub> shape memory alloy heat treated at 1000 °C for 24h (the tested alloy) in 1.0 M H<sub>2</sub>SO<sub>4</sub> solutions at the respective  $E_{corr}$  at 25 °C. Duration of the aging process is 3h.

Alloy experimental conditions	$R_s$ (kΩ cm <sup>2</sup> )	$Q$ (s <sup>n</sup> (ω <sup>-1</sup> cm <sup>-2</sup> ))	$R_{ct}$ (Ω cm <sup>2</sup> )	n	$C_{dl}$ (μF cm <sup>-2</sup> )
Tested alloy (without aging)	4.76	41.49	57187	0.87	49.21
Tested alloy after aging @ 300 °C	8.58	37.29	62228	0.89	41.38
Tested alloy after aging @ 400 °C	9.88	32.38	158850	0.92	37.33
Tested alloy after aging @ 500 °C	4.83	77.46	18995	0.83	83.83
Tested alloy after aging @ 600 °C	14.28	106.20	17500	0.78	126.48

Equation (2) provides information about the degree of non-idealibility in capacitive behavior [58]. Its value makes it possible to differentiate between the behaviour of an ideal capacitor ( $n = 1$ ) and of a constant phase element ( $n < 1$ ). Based on the above observations, the equivalent circuit depicted in Fig. 4, in which  $R_s$  is the solution resistance,  $Q$  accounts for the oxide film capacitance and double layer capacitance,  $C_{dl}$  (in series) and  $R_{ct}$  is the charge-transfer resistance, is used to fit the experimental impedance data. The value of  $C_{dl}$  can be calculated for a parallel circuit composed of a CPE( $Q$ ) and a resistor ( $R_{ct}$ ), according to the following formula [58,59]:

$$Q = (CR_{ct})^n / R_{ct} \tag{3}$$

The fitting parameters are listed in Table 2, and revealed that the  $R_{ct}$  value increases, corresponding to improved corrosion resistance, when the aging temperature is increased up to 400 °C, but decreases with further increase in the aging temperature.

At the same time the double layer capacitance ( $C_{dl}$ ) has opposite trend at the whole aging temperature range (300-600 °C). The significantly reduced impedance recorded for the alloy when aged at 600 °C afforded markedly faster charge-transfer (corrosion) process that occurred on the surface of such alloy. The reverse is true for the alloy when aged at 400 °C, which exhibited the highest  $R_{ct}$  value. These findings confirm the results obtained from the ICP-AES and polarization measurements and showed that aging our Ni<sub>52</sub>Ti<sub>47.7</sub>Re<sub>0.3</sub> shape memory alloy beyond 400 °C, up to 600 °C in this work, is harmful; it enhances the electron transfer in the system resulting in a lower semi-circle diameter which means a decrease of the charge transfer resistance at electrode surface.

The Bode phase shift plots, not included here, also gave a clear picture. The alloy when aged at 400 °C exhibited phase angles close to 90° at medium and low frequencies, suggesting the formation of compact passive film at the interface. However, upon aging the tested alloy at 600 °C, the phase angles

dropped to about  $70^\circ$  and  $55^\circ$  at medium and low frequencies, respectively. Such a behavior indicates that the passive film formed on the  $600^\circ\text{C}$  aged alloy is most probably non-protective and defective in nature.

Further inspection of Table 2 reveals that the capacitance value recorded for the alloy before aging is significantly changed upon aging, and this change varies according to the aging temperature. This difference in film capacitance could be due to the effect of aging treatment on the microstructure of our  $\text{Ni}_{52}\text{Ti}_{47.7}\text{Re}_{0.3}$  shape memory alloy [50,51]. Increasing the temperature of the aging treatment altered, as will be shown later, the microstructure of the alloy [50,51], yielding passive films with different characteristics that may affect the corrosion behavior of the tested alloy.

### 3.4. Anodic behavior of $\text{Ni}_{52}\text{Ti}_{47.7}\text{Re}_{0.3}$ SMA in 1.0 M $\text{H}_2\text{SO}_4$

#### 3.4.1. Potentiodynamic anodic polarization measurements

The effect of the aging temperature on the anodic behavior of our tested SMA was also studied, and the results obtained are depicted in Fig. 5. Measurements were conducted in 1.0 M  $\text{H}_2\text{SO}_4$  solutions at  $25^\circ\text{C}$  based on the linear sweep voltammetry technique (LSV). In all cases, the potentials were swept starting from a cathodic potential of  $-2.0\text{ V vs. SCE}$  in the anodic direction at a scan rate of  $1.0\text{ mV s}^{-1}$ . Similar findings were previously obtained in our lab during corrosion research studies on a cast Re-containing inconel 718 alloy and a Ni-base super alloy in sulphuric acid solutions [44,53].

It is obvious from Fig. 5 that on positive going scan, the cathodic current density decreases gradually and reaching a zero value at the corrosion potential ( $E_{\text{corr}}$ ). As the electrode potential was made increasingly positive, the anodic polarization curves exhibit an active/passive transition. In the active region, the dissolution current density increases linearly with the applied potential due to Ni dissolution [44,53].

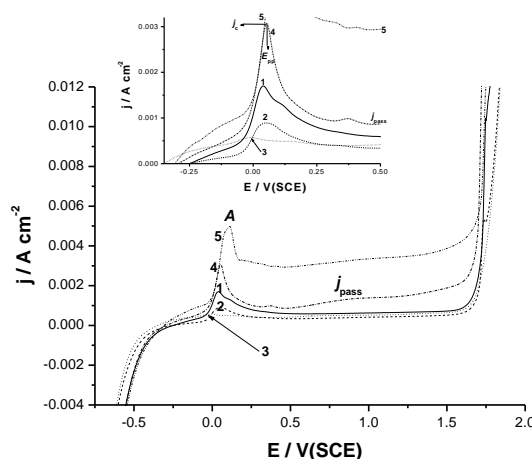


**Figure 5.** Potentiodynamic anodic polarization curves recorded for  $\text{Ni}_{52}\text{Ti}_{47.7}\text{Re}_{0.3}$  shape memory alloy in 1.0 M  $\text{H}_2\text{SO}_4$  solutions at a scan rate of  $1.0\text{ mV s}^{-1}$  at  $25^\circ\text{C}$  as a function of the temperature of the aging treatment. The alloy is first solution treated at  $1000^\circ\text{C}$  for 24h (curve 1), then aged at various temperatures of 300, 400, 500 and  $600^\circ\text{C}$  for 3h, curves 2-5, respectively.

This is followed by the appearance of the anodic peak A. The decay in the active dissolution current density is related to the formation of a protective oxide film. Therefore, the appearance of peak A is indicative of two processes; metal dissolution and subsequent formation of soluble complex species and the formation of a protective passive film. The anodic dissolution current density drops to a very small value, designated as passive current ( $j_{\text{pass}}$ ), indicating the onset of passivation. The value of  $j_{\text{pass}}$  is limited by the chemical dissolution of the film. The chemical film dissolution is counterbalanced by film formation. The rates of these two processes are nearly the same at the steady-state of polarization so as to keep the thickness of the passive film nearly constant.

Further inspection of Fig. 5 reveals that the tested alloy exhibited almost the same active to passive transition behavior whatever the aging temperature. However, the anodic behavior of these materials was quite different in terms of the critical anodic current density required for passivation ( $j_c$ ), the primary passive potential ( $E_{\text{pp}}$ ), the passive current density ( $j_{\text{pass}}$ ), see the inset of Fig. 5, and the extent of the passive region. It is clear that both  $j_c$  and  $j_{\text{pass}}$  (at any given potential within the passive region) enhance following the order: 400 °C aged alloy < 300 °C aged alloy < the tested alloy (that is solutionized, but not aged) < 500 °C aged alloy < 600 °C aged alloy. When aged at 400 °C, the tested SMA recorded the lowest  $j_c$  and  $j_{\text{pass}}$  values. In addition, it exhibited the widest passive region. These findings support previous uniform corrosion studies (Figs. 1-3) and reflects the highest corrosion resistance of the tested alloy when aged at 400 °C. At the end of the passive region (beyond 1.5 V), the anodic current increases rapidly with increasing potential and gas evolution is observed. A number of microscopic pits were observed on the surface after this polarization. This was attributed to both the transpassive dissolution of NiTi and the oxygen evolution taking place heterogeneously on the surface [60].

### 3.4.2. Chronoamperometry measurements

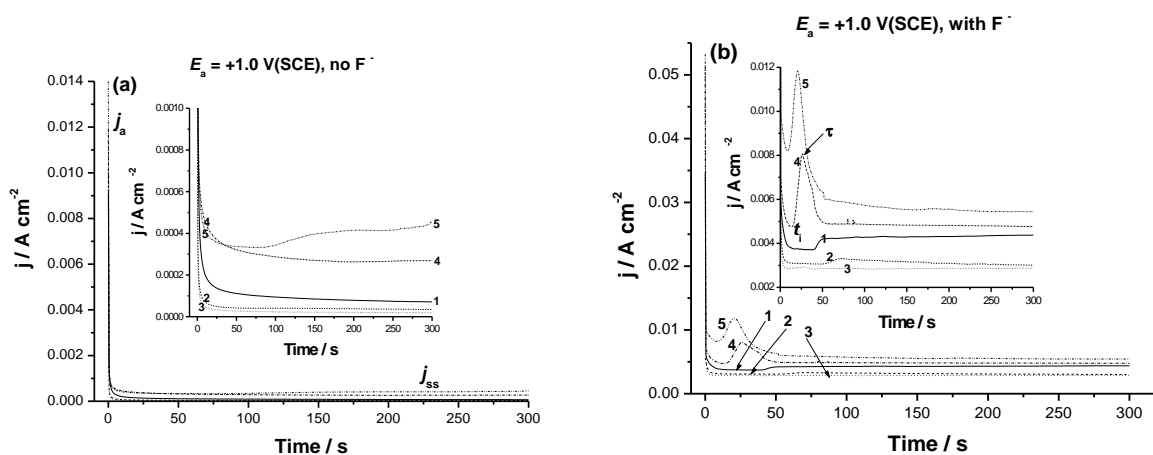


**Figure 6.** Chronoamperometry measurements recorded for Ni<sub>52</sub>Ti<sub>47.7</sub>Re<sub>0.3</sub> shape memory alloy in 1.0 M H<sub>2</sub>SO<sub>4</sub> solutions (a) without and (b) with 0.2 M NH<sub>4</sub>F at a fixed anodic potential ( $E_a$ ) of 1.0 V(SCE) at 25 °C as a function of the temperature of the aging treatment. The alloy is first solution treated at 1000 °C for 24h (curve 1), then aged at various temperatures of 300, 400, 500 and 600 °C for 3h, curves 2-5, respectively.

Chronoamperometry (current vs. time) measurements were also carried out to gain more information about the effect of aging temperature on the kinetics of passive layer growth and its breakdown (pitting corrosion). In this respect, measurements were performed in 1.0 M H<sub>2</sub>SO<sub>4</sub> solutions without and with 0.2 M NH<sub>4</sub>F at a fixed anodic potential of 1.0 V (SCE), as shown in Fig. 6. It is seen that, in absence of F<sup>-</sup> (Fig. 6a), the transient current profile can be divided into two stages. In the first stage, the anodic current transient decreases rapidly with time, due to the electroformation and growth of a passive oxide film on the anode surface [62,63].

The anodic current of the second stage (steady-state current,  $j_{ss}$ ) was nearly constant irrespective of applied potential, indicating that the rate of oxide formation equals that rate of oxide dissolution so that the oxide film hardly grows [44,62,63]. In such a case, the overall transient current density can be related to two main processes, namely the passive layer growth ( $j_{gr}$ ) and metal electrodissoolution through the passive layer ( $j_{dis}$ ), Eq. 4.

$$j = j_{gr} + j_{dis} \quad (4)$$

The growth of the passive layer can be assigned to the formation of a passive oxide solid phase on the electrode surface. The electrodissoolution of the anode through the passive layer can be explained in terms of cation diffusion from the metal/film interface to the film/solution interface [63]. These two processes can proceed independently on the entire electrode surface. It seems that the rates of these two processes are nearly the same at the steady-state current so as to keep the thickness of the passive film nearly constant [62,63]. It is observed that the value of  $j_{ss}$  decreases, corresponding to a more protective passive oxide film, as the aging temperature is increased up to 400 °C. On the other hand, the value of  $j_{ss}$  enhances when the tested SMA is aged at 500 °C (curve 4) and 600 °C (curve 5), reflecting the formation of a less protective (thin and/or porous) passive film.

Referring again to Fig. 6a, it is clear that the tested alloy exhibited the slowest decay of  $j_a$ , which is related to an increased dissolution at the early stages [64], when aged at 600 °C (curve 5), reflecting its low corrosion resistance. The reverse is true for 400 °C aged alloy (curve 3), which exhibited the fastest decay of  $j_a$ . These findings mean that the tested SMA exhibited the fastest passivation rate (i.e., rapid decay of  $j_a$  and low dissolution rate) when aged at 400 °C; the reverse is true for aging at 600 °C.

In presence of F<sup>-</sup> (Fig. 6b), the overall process can be divided into the three stages, namely the first passivation stage, the second pit formation and growth stage and the final steady-state stage (observed for the tested alloy without aging, curve 1, and for the tested alloy after aging at 300 °C, curve 2) and the final current decay (re-passivation) stage, recorded for 500 °C and 600 °C aged alloys (curves 4 and 5). The 3<sup>rd</sup> stage is completely absent when the alloy is aged at 400 °C (curve 3), reflecting its high corrosion resistance. The anodic current density of the first stage descended abruptly with time and then reached a current minimum at a certain incubation time,  $t_i$ . The incubation time is caused by the time required for local removal of the passive film via the sequence of F<sup>-</sup> adsorption, penetration and formation of soluble complexes [63,64]. The fall of current density indicates thickening of oxide film on the surface. In the second stage, the value of current density ascended from the moment just after  $t_i$  to another time designated here as  $\tau$ , which is attributed to passivity breakdown induced by the aggressive attack of F<sup>-</sup>, and subsequent formation and growth of pits [64].

Within the 2<sup>nd</sup> stage, the general trend of an increasing current suggests that pit growth is the dominant process and a number of well-developed pits could be observed following this active period. In this case, the overall transient current density is given by three contributions, Eq. 5, with  $j_{\text{pit}}$  being related to the pit growth current density.

$$j = j_{\text{gr}} + j_{\text{dis}} + j_{\text{pit}} \quad (5)$$

After pit initiation and growth has been completed, i.e., at the end of the 2<sup>nd</sup> stage, where  $j_{\text{pit}}$  reached its maximum value,  $j_{\text{pit}}$  starts to fall, denoting the onset of the 3<sup>rd</sup> stage. It is possible that pitting corrosion products and/or metal oxides layers precipitate inside the pits, and as the reaction proceeds form on the entire surface. Such layers possess some protective influence; block up the pits, and therefore hinder the current flow through the pits, thus reducing the active dissolution of the alloy. This surface blockade by pitting corrosion products may be the main reason behind the current fall in the 3<sup>rd</sup> stage [64].

The events of the 3<sup>rd</sup> stage were happened to the tested alloy when aged at 500 °C and 600 °C (curves 4 and 5), as such high aging temperatures enhanced alloy corrosion, helping it form corrosion products on its surface. On the other hand, the surface of the tested alloy when aged at 400 °C (curve 3) lacks corrosion products due to the high corrosion resistance the alloy exhibited when aged at that temperature. The alloy when aged at 300 °C (curve 2) showed a trend similar to that of the tested alloy itself (that is not aged, curve 1); the 3<sup>rd</sup> stage of which is characterized by a steady current. Within the 3<sup>rd</sup> stage of curves 1 and 2, the increment in current density caused due to the metal dissolution just equals the sum of the decrement in current density due to oxide film formation and the decrement of current density due to the blockade by pitting corrosion product, leading to nearly constant current density. Similar findings were previously obtained in our lab [44,62-65].

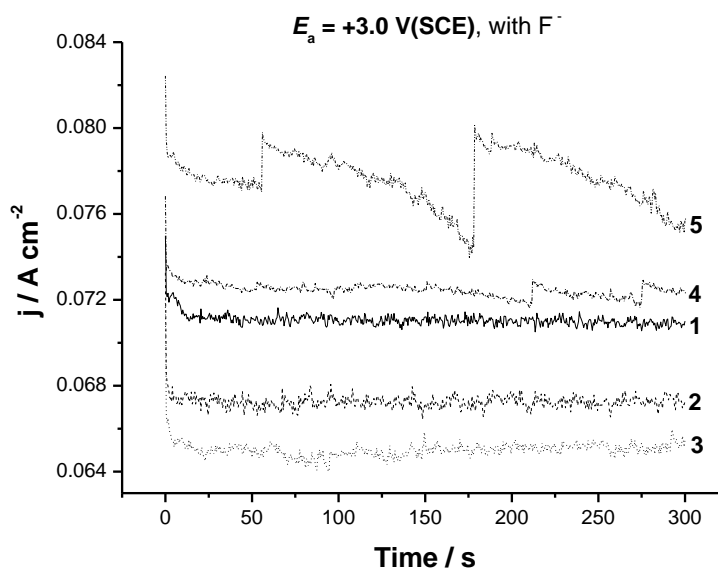


**Figure 7.** Chronoamperometry measurements recorded for Ni<sub>52</sub>Ti<sub>47.7</sub>Re<sub>0.3</sub> shape memory alloy in 1.0 M H<sub>2</sub>SO<sub>4</sub> solutions (a) without and (b) with 0.2 M NH<sub>4</sub>F at a fixed anodic potential ( $E_a$ ) of 1.0 V(SCE) at 25 °C as a function of the temperature of the aging treatment. The alloy is first solution treated at 1000 °C for 24h (curve 1), then aged at various temperatures of 300, 400, 500 and 600 °C for 3h, curves 2-5, respectively.

Chronoamperometry measurements have also been carried out at higher anodic potentials, 3.0 V(SCE), Fig. 7. It is seen that the passive state is interrupted by current fluctuations due to metastable pitting [63]; a point of research that deserves complementary studies. Similar findings were obtained by Middleton et al. on titanium corrosion [66], by Gupta et al. in aluminum alloys [67], and in our lab by on aluminum and zinc corrosion [64,68], using solutions containing chlorides.

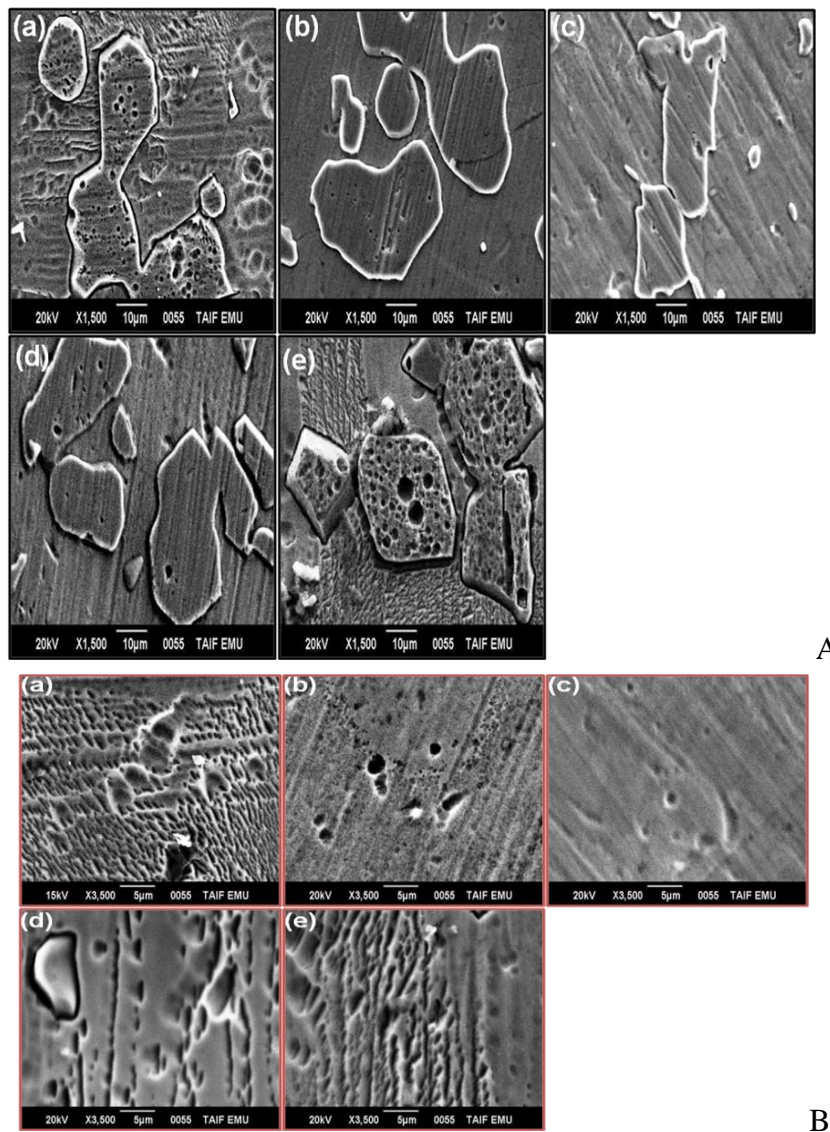


**Figure 8.** SEM micrographs recorded for  $Ni_{52}Ti_{47.7}Re_{0.3}$  shape memory alloy after holding the alloy at a constant anodic potential of 3.0 V(SCE) for 5.0 minutes. Measurements were conducted in (1.0 M  $H_2SO_4$  + 0.2 M  $NH_4F$ ) solution at 25 °C as a function of aging temperature. (a) The alloy is heat treated at 1000 °C for 24h, but not yet aged. After being heat treated, the alloy is aged at various temperatures of 300, 400, 500 and 600 °C for 3h, **images b-e**, respectively. Series (A): to show pitting corrosion of precipitates, and (B) to clarify susceptibility of the matrix towards pitting.

Figure 7 also shows that the background passive current  $j_{ss}$ , and hence the alloy dissolution rate [64], diminishes with aging temperature up to 400 °C (compare curves 2 and 3 with curve 1), but

enhances with further increase in the aging temperature, curves 4 and 5. Also, the height and the frequency of current spikes vary according to aging temperature. Current spikes with maximum height and the frequency are observed when the alloy is aged at 600 °C, curve 5, and weak current spikes were recorded for the alloy when aged at 300 °C and 400 °C, curves 2 and 3, respectively. These findings point to the high pitting corrosion resistance the tested SMA exhibited when aged at 400 °C.

After chronoamperometry measurements (Fig. 7) have been completed, morphologies of the pitted surfaces were investigated. The obtained SEM images are depicted in Fig. 8 as a function of aging temperature. Pitting corrosion attack induced by  $F^-$  on both the precipitates, Fig. 8A, and matrix, Fig. 8B, can be observed in all tested samples, the severity of which varies with the aging temperature. While the surfaces of the tested alloy (without aging), Fig. 8A (image a), and that aged at 500 °C and 600 °C (Fig. 8, images d and e) exhibited the highest susceptibility towards pitting corrosion, a less pronounced pitting attack was observed on the alloy surface aged at 300 °C (Fig. 8, images b) and 400 °C (Fig. 8, images c). Pitting attack is also evident on the matrix surface (Fig. 8B), the severity of which diminishes upon aging up to 400 °C (Fig 8B, images b and c), then obviously enhances with further increase in the aging temperature up to 600 °C, (Fig 8B, images d and e). These results support chronoamperometry measurements (Fig 7), and indicate that our tested shape memory alloy exhibited the highest pitting corrosion resistance when aged at 400 °C, but becomes more susceptible to pitting with further increase in the aging temperature.

### 3.5. Aging temperature, microstructure and corrosion behavior

Experimental findings of the present work revealed that the corrosion behavior of our tested  $Ni_{52}Ti_{47.7}Re_{0.3}$  SMA obviously varies with aging temperature. Our research group has recently studied the influence of the aging treatment on the microstructure of  $Ni_{52}Ti_{47.7}Re_{0.3}$  SMA [50,51], and reported that increasing the aging temperature from 300 °C up to 600 °C has significantly altered the microstructure of the tested SMA. Therefore, experimental corrosion data reported here can be interpreted adopting the effect of the aging treatment on the microstructure of the tested sample [50,51]. It has been shown that the microstructure of solutionized and aged alloys consists of martensite (B19') as a parent phase in addition to precipitates of  $Ti_2Ni$  phase in two shapes; the first is fine irregular circular shape, while the second one is blocky agglomerated precipitate [50,51]. In addition to the precipitates of  $Ti_2Ni$  phase, elevating the aging temperature to 500 °C has resulted in the formation of a new Ti-rich precipitate, namely  $Ti_4Ni_3$ . Besides  $Ti_2Ni$  and  $Ti_4Ni_3$  phases, additional aging heat treatments at 600 °C formed a new Ni-rich phase ( $Ni_3Ti$ ) [50,51].

The good corrosion resistance of NiTi results from the formation of very stable, continuous, highly adherent, and protective oxide films on its surface. Because titanium is highly reactive and has a high affinity for oxygen, these beneficial surface oxide films form spontaneously when fresh metal surfaces are exposed to air and/or moisture. The high Ni content of the alloy is also expected to contribute with Ti in protecting the alloy against corrosion via the formation of a protective passive film of Ni oxide [50,51]. Thus depletion of Ni and Ti from the alloy matrix will weaken the passive layer and enhance corrosion. The formation of  $Ti_2Ni$ ,  $Ti_4Ni_3$ , and  $Ni_3Ti$  precipitates are expected to

exert a significant negative influence on the corrosion resistance of the tested alloy, as they lead to the depletion of Ni and Ti from the matrix. These harmful phases (from the corrosion point of view) accelerate corrosion to an extent depend on their content (measured by the volume fraction,  $V_f$ ) in the alloy, which in turn depends on the aging temperature.

The aged alloy with the lowest  $V_f$  of precipitates is expected to be the most corrosion resistant. It has been shown that upon increasing aging temperature,  $V_f$  of  $Ti_2Ni$  precipitates in the microstructure decreases due dissolution of precipitates into the matrix [51]. This is the reason why the alloy when aged at 600 °C recorded the lowest  $V_f$  value for the precipitates of  $Ti_2Ni$ , but the highest  $V_f$  value for  $Ti_2Ni$  is obtained when the aging process is carried out at 300 °C [51]. However, the  $Ti_4Ni_3$  and  $Ni_3Ti$  phases additionally formed in the microstructure of the 600 °C aged alloy resulted in an obvious increase in its  $V_f$  [51]. It was concluded that the alloy when aged at 400 °C recorded the lowest  $V_f$  value, as it contains only  $Ti_2Ni$  precipitates in its microstructure, but the highest  $V_f$  value is obtained upon elevating the aging temperature up to 600 °C, where three types of precipitates;  $Ti_2Ni$ ,  $Ti_4Ni_3$  and  $Ni_3Ti$  are formed [51]. The high volume fraction of the precipitates of the 600 °C aged alloy may be the main reason behind its low corrosion resistance in  $H_2SO_4$  solutions. In addition, the multiphase structure of the 600 °C aged alloy may create galvanic cells, which in turn enhance the corrosion process.

#### 4. CONCLUSIONS

The uniform corrosion characteristics of  $Ni_{152}Ti_{47.7}Re_{0.3}$  SMA (subjected to solution treatment at 1000 °C for 24h) were investigated as a function of aging temperature (300 °C – 600 °C). Measurements were conducted in 1.0 M  $H_2SO_4$  solutions, based on monitoring open-circuit potential (OCP), Tafel extrapolation and impedance methods. An independent method of chemical analysis, namely ICP-AES (inductively coupled plasma atomic emission spectrometry) was also used to test validity of corrosion rate measured by Tafel extrapolation method. ICP-AES method confirmed the validity of Tafel extrapolation method for monitoring corrosion rates and revealed that the uniform corrosion rate decreased with increase in the aging temperature up to 400 °C, then decreased with further elevation in the aging temperature. EIS spectra measured at  $E_{corr}$  came to the same conclusion and showed that the total impedance ( $Z$ ) increased with aging temperature, but decreased with further increase in aging temperature. In this respect, our tested SMA alloy aged at 400 °C recorded the lowest uniform corrosion rate, while the highest corrosion rate was reported for the alloy when aged at 600 °C.

The anodic behavior and the kinetics of passive layer growth and its breakdown was also studied in  $NH_4F-H_2SO_4$  containing solutions as a function of the aging, employing potentiodynamic anodic polarization and chronoamperometry measurements. Results showed that the susceptibility of the tested SMA towards pitting attack (induced by  $F^-$ ) was suppressed upon increasing aging temperature from 300 to 400 °C, but enhanced with further increase in aging temperature. Here also, the alloy recorded its lowest rate of pit initiation and growth when aged at 400 °C. On the other hand, that alloy exhibited the highest rate of pit initiation and growth when the aging treatment was carried

out at 600 °C. Morphological studies, based on SEM examinations, came to the same conclusion and revealed that the 400 °C aged alloy exhibited the lowest severity of pitting attack. The reverse is true for the 600 °C aged alloy.

## References

1. A. Ölander A. *Am. Chem. Soc.*, 54 (1932) 3819.
2. L.B. Vernon, H.M. Vernon, Process of manufacturing articles of thermoplastic synthetic resins. In: US Patent 2234993; 1941.
3. W.J. Buehler, J.V. Gilfrich, R.C. Wiley, *Appl. Phys.*, 34 (1963) 1475.
4. G. Kauffman, I. Mayo, *Chem. Educator*, 2 (1997) 1.
5. M.H. Wu, L.M. Schetky, Industrial applications for shape memory alloys. In: International conference on shape memory and superelastic technologies. Pacific Grove, California, USA; 2000. p. 171–82.
6. R.B. Zider, J.F. Krumme, Eyeglass frame including shape-memory elements. In: US Patents 4772112. Menlo Park, California, USA: CVI/Beta Ventures, Inc.; 1988.
7. A. Hautcoeur, A. Eberhardt, Eyeglass frame with very high recoverable deformability. In: US Patents 5640217. Fergaflex, Inc., Montreal, Canada; 1997.
8. Y. Furuya, *Intell. Mater. Syst. Struct.*, 7 (1996) 321.
9. H. Wu, L.M. Schetky, Industrial applications for shape memory alloys, Proceedings of the International Conference on Shape Memory and Superelastic Technologies, Pacific Grove, California, P.171-182 (2000), and references therein.
10. D. Stoeckel, *Mat. Des.*, 11 (1990) 302.
11. C. Bil, K. Massey, E.J. Abdullah, *J. Intell. Mater. Syst. Struct.*, 24 (2013)879.
12. D.J. Hartl, D.C. Lagoudas, *J. Aerospace. Eng.*, 221 (2007) 535.
13. J.V. Humbeeck, *Mater. Sci. Eng.*, A 134 (1999) 134.
14. S.L. McDonald, *Mater. Des.*, 12 (1991) 29.
15. L. Sun, W.M. Huang, Z. Ding, Y. Zhao, C.C. Wang, H. Purnawali, *Mater. Des.*, 33 (2012) 577.
16. M. Kohl, Shape memory microactuators (microtechnology and MEMS). 1 ed. Heidelberg: Springer-Verlag Berlin; 2010.
17. H. Kahny, M.A. Huffz, A.H. Heuer, *Micromech. Microeng.*, 8 (1998) 213.
18. H. Fujita, H. Toshiyoshi, *Microelectron. J.*, 29 (1998) 637.
19. M. Kheirikhah, S. Rabiee, M. Edalat, A review of shape memory alloy actuators in robotics. In: Ruiz-del-Solar J, Chown E, Ploger P, editors. RoboCup 2010: Robot Soccer World Cup XIV. Berlin Heidelberg: Springer; 2011. p. 206–17.
20. M. Sreekumar, T. Nagarajan, M. Singaperumal, M. Zoppi, R. Molfino, *Ind Rob.: Int. J.*, 34 (2007) 285.
21. Y. Furuya, H. Shimada, *Mater Des* 12 (1991) 21.
22. L.V. Langenhove, C. Hertleer, *Int. J. Clothing Sci. Technol.*, 16 (2004) 63.
23. K. Wilkes, P. Liaw, K. Wilkes, *JOM* 52 (2000) 45.
24. J. Cederström, J.V. Humbeeck, *J. Phys. IV France* 5 (1995) C2-335-C2- 41.
25. D.E. Hodgson, M.H. Wu, R.J. Biermann, Shape memory alloys. *ASM Handbook: ASM International* 1990:897–902.
26. W. Huang, *Mater. Des.*, 23 (2002) 11.
27. L. Petrini, F. Migliavacca, *J. Metall.*, 2011(2011) 1.
28. C. Song, *Open Med. Dev. J.*, 2 (2010) 24.
29. N.B. Morgan, *Mater. Sci. Eng. A*, 378 (2004) 16.
30. L.G. Machado, M.A. Savi, *Braz. J. Med. Biol. Res.*, 36 (2003) 683.
31. D. Mantovani, *JOM* 52 (2000) 36.

32. T. Duerig, A. Pelton, D. Stockel, *Mater. Sci. Eng. A*, 273-275 (1999) 149.
33. R.P. Frankenthal, J. Kruger (Eds.), Passivity of Metals, *Electrochem. Soc. Princeton, NJ* (1978), p. 165.
34. H.J. Jang, C.J. Park, H.S. Kwon, *Electrochim. Acta* 50 (2005) 3503.
35. G. Frankel, *J. Electrochem. Soc.* 145 (1998) 2186.
36. O.M. Magnussen, J. Scherer, B.M. Ocko, R.J. Behm, *J. Phys. Chem. B* 104 (2000) 1222.
37. N. Pineau, C. Minot, V. Maurice, P. Marcus, *Electrochem. Solid-State Lett.* 6 (2003) B47.
38. A. Bouzoubaa, B. Diawara, V. Maurice, C. Minot, P. Marcus, *Corros. Sci.* 51 (2009) 2174.
39. S. Singh, S. Basu, A.K. Poswal, R.B. Tokas, S.K. Ghosh, *Corros. Sci.* 51 (2009) 575.
40. T. Nickchi, A. Alfantazi, *Corros. Sci.*, 52 (2010) 4035.
41. A. Bloyce, P.Y. Qi, H. Dong, T. Bell, *Surf. & Coat. Technol.*, 107 (1998) 125.
42. X.D. Lu, H.M. Wang, *J. Alloys and Compds.*, 465 (2008) 83.
43. Q. Bi, W. Liu, J. Ma, J. Yang, Y. Pu, Q. Xue, *Tribology International* 42 (2009) 1081
44. M.A. Amin, N. El-Bagoury, M. Saracoglu, M. Ramadan, *Int. J. Electrochem. Sci.*, 9 (2014) 5352.
45. A. Phukaoluan, A. Khantachawana, S. Dechkunakorn, N. Anuwongnukroh, P. Santiwong, Julathep Kajornchaiyakul, *Advanced Materials Research*, 378 – 379 (2011) 650.
46. E. Kassab, L. Neelakantan, M. Frotscher, S. Swaminathan, B. Maaß, M. Rohwerder, J. Gomes and G. Eggeler, *Mater. and Corros.*, 65 (2014) 18.
47. C. Craciunescu, A. Hamdy, *Int. J. Electrochem. Sci.*, 8 (2013) 10320.
48. M.A. Amin, N. El-Bagoury, A.A. Omar, A.S. Megahed, *Int. J. Electrochem. Sci.*, 7 (2012) 2643.
49. N. El-Bagoury, M.A. Amin, H. Shokry, *Int. J. Electrochem. Sci.*, 8 (2013) 1246.
50. N. El-Bagoury, M.M. Hessien, Z. I. Zaki, *Met. Mater. Int.* 20 (2014) 997.
51. N. El-Bagoury, *Mater. at High Temp.*, 2014, In Press Corrected Proof.
52. E. McCafferty, *Corros. Sci.* 39 (1997) 243.
53. ASTM G 102 – 89 (Reapproved 1999), Standard Practice for Calculation of Corrosion Rates and Related Information from Electrochemical Measurements.
54. N. El-Bagoury, M.A. Amin, Q. Mohsen, *Int. J. Electrochem. Sci.*, 6 (2011) 6718.
55. M. Metikos-Hukovic, R. Babic, Z. Grubac, *J. Appl. Electrochem.* 32 (2002) 35.
56. F. Mansfeld, *Corrosion* 37 (1981) 301.
57. M. Metikos-Hukovic, R. Babic, Z. Grubac, S. Brinic, *J. Appl. Electrochem.* 26 (1996) 443.
58. X. Wu, H. Ma, S. Chen, Z. Xu, A. Sui, *J. Electrochem. Soc.* 146 (1999) 1847.
59. H. Ma, S. Chen, B. Yin, S. Zhao, X. Liu, *Corros. Sci.* 45 (2003) 867.
60. K. Fushimi, M. Stratmann, A.W. Hassel, Electropolishing of NiTi shape memory alloys in methanolic H<sub>2</sub>SO<sub>4</sub>, *Electrochim. Acta* 52 (2006) 1290–1295.
61. M.A. Amin, S.S. Abd El Rehim, S.O. Moussa, A.S. Ellithy, *Electrochim. Acta*, 53 (2008) 5644.
62. S.S. Abdel Rehim, H.H. Hassan, M.A. Amin, *Corros. Sci.*, 46 (2004) 1921.
63. M.A. Amin, S.S. Abd El-Rehim, F. D. A. Araújo Reis, I. S. Cole, *Ionics* 20 (2014) 127.
64. M.A. Amin, S.S. Abd El-Rehim, E.E.F. El-Sherbini, S.R. Mahmoud, M.N. Abbas, *Electrochim. Acta*, 54 (2009) 4288.
65. Z. Jiang, T. Norby, H. Middleton, *Corros. Sci.*, 52 (2010) 3158.
66. R.K. Gupta, N.L. Sukiman, M.K. Cavanaugh, B.R.W. Hinton, C.R. Hutchinson, N. Birbilis, *Electrochim Acta* 66 (2012) 245.
67. M.A. Amin, *Electrochim. Acta* 54 (2009) 1857.